

# **Study of Current Ripple Generators for Accelerated Ageing of Capacitors**

Robert Keilmann<sup>1</sup>, Hendrik Schefer<sup>1,2</sup>, Regine Mallwitz<sup>1,2</sup>

INSTITUTE FOR ELECTRICAL MACHINES, TRACTION AND DRIVES (IMAB)<sup>1</sup>

CLUSTER OF EXCELLENCE SE<sup>2</sup>A – SUSTAINABLE AND ENERGY-EFFICIENT AVIATION<sup>2</sup>

TU Braunschweig

Braunschweig, Germany

E-Mail: h.schefer@tu-braunschweig.de

URL: <https://www.tu-braunschweig.de/imab>

URL: <https://www.tu-braunschweig.de/se2a>

## **Acknowledgements**

This work was supported by the Deutsche Forschungsgemeinschaft (German Research Foundation, DFG) through Germany's Excellence Strategy-EXC 2163/1-Sustainable and Energy Efficient Aviation under Grant 390881007.

## **Keywords**

«Test bench», «Reliability», «Passive component», «Resonant converter», «Wide bandgap devices»

## **Abstract**

Upcoming developments in aerospace power applications demand the use of WBG semiconductors. They offer higher switching frequencies resulting in high-frequency ripple currents in the DC-link. These currents may lead to excessive stress on the DC-link capacitors. This paper proposes a modular ripple current generator for the accelerated ageing of capacitors using high-frequency ripple currents.

## **I Introduction**

Research shows that many applications benefit from the use of fast-switching, wide bandgap (WBG) semiconductors. There are countless studies on the use of novel semiconductors in grid feed applications. This especially includes renewable energy systems like photovoltaics and wind turbines respectively wind parks. But there are also mobile applications that benefit from the use of WBG semiconductors. These are, for example, electrified cars and trains. The scope of current research also includes applications in the aviation sector. Researchers found that using WBG semiconductors might be advantageous for all-electric aircraft [1].

Capacitors are critical components that are frequently affected by failures [2]. Therefore, the studies of [3], [4] or standards such as EIA IS-749 provide guidance to develop power electronics with lifetime based approaches as well as to induce accelerated ageing. A novel way to approach a variety of test frequencies using a modular concept will be shown to induce accelerated ageing under challenging climatic conditions for different capacitor types.

This paper is structured as follows. Section II discusses the ageing mechanisms known from the literature for the types of capacitors typically used in power electronics. Section III illustrates the overall problem using the example of a three-phase inverter and describes two approaches for the targeted accelerated ageing of capacitors. In Section IV, the advantages and disadvantages of three circuit variants for generating ripple currents are worked out in a topology study. Section V specifies the method and devised approach of the modular and flexible series resonant converter. Section VI deals with the parameters

influencing the overall system as well as the design rules of the ripple current generator. The working prototype is presented in section VII. The fact that first studies have been successfully carried out with the novel approach is then illustrated in conclusion in section VIII.

## II Ageing of Capacitors

Aluminium-Electrolytic-Capacitor (Al-Caps), Metallized-Polypropylene-Film Capacitors (MPPF-Caps) and Multi-Layer-Ceramic-Capacitors (MLC-Caps) have different voltage ratings and capacity ranges; therefore, various possible use-cases. The paper [4] compares these capacitor types against each under three relative performance indices.

Aircraft applications require different types of capacitors and their properties. There is no capacitor type for all kinds of converters and inverters. Furthermore, co-existences in DC-links are often required. The substitution of conventional propulsion systems in aircraft needs high voltage ranges, high energy densities and high frequencies under high-reliability requirements [1].

Table I summarizes the external stress factors of the chosen capacitor types. Al-Caps have reliability-related issues to electrolyte evaporation driven by thermal conditions, self-heating mechanism (ripple current and ESR) and normal ageing [4]. The applied DC voltage exerts dielectric stress [4]. Mechanical stress can lead to electrical disconnections [5]. MPPF-Caps have an additional lifetime-related parameter. There is reversible and irreversible humidity absorption [4]. Over a humidity-exposure time, degradation of metallised layers occurs [6]. In the dielectric of MLC-Caps, there can occur some ceramic micro-cracking due to mechanical oscillations [7].

Table I: Capacitor Stress Focus Point Matrix based on [4]

	Al-Caps	MPPF-Caps	MLC-Caps
Critical Stressors	Voltage, Temperature, Ripple Current		
	Vibration	$\frac{dU}{dt}$ , Humidity	Vibration/Shock
Most Critical Stressors	Voltage and Temperature		
	Ripple Current	Humidity	Vibration/Shock

The replication of the stress factors requires a current ripple generator with temperature, voltage, and humidity adjustment opportunities. Mechanical stress is not taken into account. The number of stress factors necessitates the design of experiments; therefore, it requires many test slots for different test conditions and statistical significance.

## III Approaches for test benches and definition of requirements

Depending on the target topology, different current characteristics occur in capacitors. The current shapes differ, the amplitudes are largely determined by the required power and the difference between the input voltage and output voltage. A 100kW inverter with a 50kHz switching frequency serves as an illustration. The ripple current depends on many parameters, such as modulation degree  $M$ , power factor  $\cos\varphi$ , line frequency  $f_s$ , the number of parallel-switched capacitor strings, etc. The publication [8] shows analytical equations to calculate the root-mean-square DC-link ripple current  $I_{c,rms}$  for a three-phase inverter system. Eight capacitor strings lead to a per-string current  $I_{c,rms} = 8.4\text{A}$  at the doubled order of the switching frequency  $f_\mu = 100\text{kHz}$ .

To obtain information about the expected service life of the capacitors used, they can be subjected to accelerated ageing in the laboratory. In the literature, two possibilities are usually shown for how to generate ripple currents for accelerated ageing. On the one hand, it is possible to actively induce a current into the capacitor [9] which represents a topology-independent approach. A differing approach is the targeted-topology approach where the capacitor is operated in the target topology directly [10].

## A Targeted-Topology Approach

This method [10] offers the advantage that the expected current waveforms and amplitudes occur and the capacitor undergoes the same ageing processes in the laboratory as it does in the field. But this method has also several disadvantages.

A practical disadvantage arises in target applications with high power ratings. Here, an electronic load is needed where electric energy is being fed back into the grid or the DC-link. Especially, multi-phase AC inverters require multi-phase loads with massive filter efforts. In [11] this problem is mitigated by the use of a scaled-down version of the inverter. There, the DC-link capacitor is exposed to a high DC-link voltage and high ripple currents in a very similar manner to the full-scale inverter. Due to the scaling, the miniature inverter in [11] has a power rating of 640 VA instead of the full-scale version with a power rating of 6400 VA.

Secondly, one is now restricted to a single topology. This means that systematic testing of different capacitors for a wide range of applications and topologies is not possible. Additionally, accelerated testing could be limited to power electronic housing. A crucial parameter is humidity for MPPF-caps, as mentioned above in Table I. Other electronic components have to withstand the conditions in a case of an open power electronic housing. To extend the DC-link outside the electronic housing is not a good solution because an additional impedance leads to unrealistic waveforms. Fig. 1 illustrates a possible approach. Here, the power electronics are positioned in a climate chamber. It can be addressed, controlled and monitored during operation via appropriate interfaces. The power electronics located in the climate chamber must be connected to a high-voltage source and the load via a suitable cable connection. If water cooling is required, supply lines to the chiller provided for this purpose must be implemented.

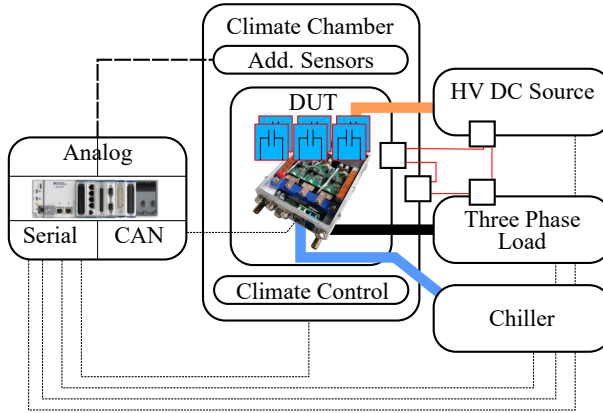


Fig. 1: Topology-dependent approach for accelerated ageing of components

## B Topology-independent Approach

In own studies, the possibility to induce the real ripple currents (example: trapezoidal, triangle, etc.) of the DC-link capacitor according to the real waveforms and amplitudes was investigated. For this purpose, investigations and efforts were made to develop a push-pull output stage (Class G Amplifier) capable of reproducing the expected DC-link capacitor currents in shape and amplitude. However, limitations quickly arise here that prevent use in the intended form.

## IV Topology Study

In advance, three circuit types were subjected to a topology study. Namely, these are the Push-Pull Output Stage (Class G Amplifier), Class D Amplifier and the Series Resonant Converter (see Fig. 2 a-c)). Table II illustrates their main characteristics.

The Class G Amplifier's ability to amplify arbitrary waveforms is advantageous. This amplifier has a higher efficiency than the Class A, Class B or Class AB amplifier [12]. As mentioned above, in a practical design study a Class G Amplifier was designed with high dynamics and power ratings to recreate the

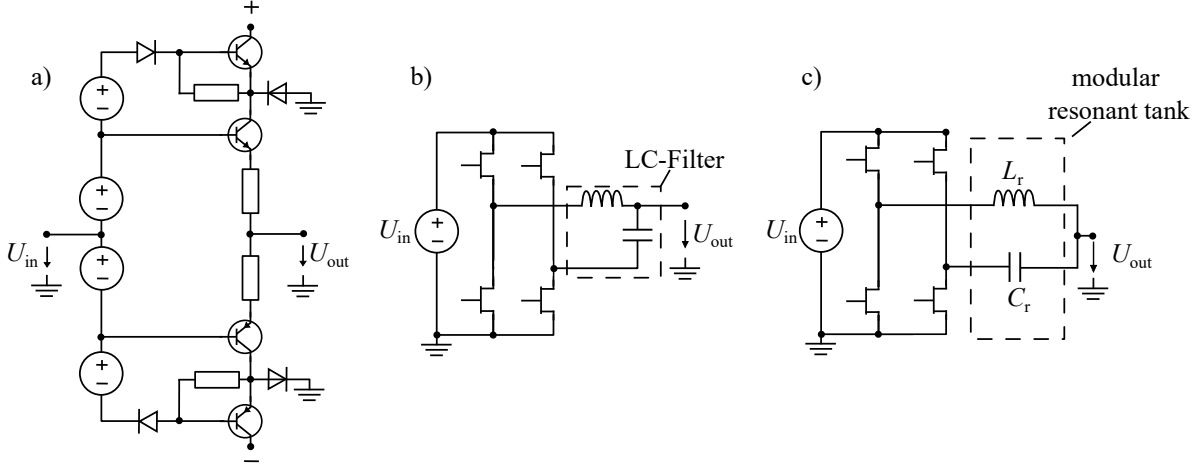


Fig. 2: From left to right: a) Push-Pull Output Stage, b) Class D Amplifier, c) Series Resonant Converter

real waveforms that occur at the DC-link. It was found that the averaged power dissipation in the output stage transistors is in the range of 385 W. Thus, a water cooling would be necessary and in the context of a statistical study, where multiple ripple current generators have to be operational for a long period of time, high energy costs would be inevitable due to the high power losses. It was also found that the cable and transformer impedances have the consequence that originally sharp edges in the waveforms are being smoothed out. With these findings in mind, it must be concluded that the Class G Amplifier is not suitable as a ripple current generator.

As an alternative, the Class D Amplifier shifts into focus. Its switching semiconductors promise higher efficiency but also make an output filter necessary. At first glance, this topology seems very advantageous. The frequencies could simply be specified via software. To reduce the EMC difficulties that come with this topology at least a filter second order is recommended [12]. There are major challenges in the dimensioning of this output filter, since it depends on the load impedance [12]. The proposed Class D Amplifier in [13] delivers an output power of 300 W at an output signal frequency of 13.56 MHz. For this, the output filter is a resonant circuit with fixed and known values for the resonant inductance  $L$ , resonant capacitance  $C$  as well as a load resistance  $R_L$ . Also [13] approaches a high-frequency Class D Amplifier delivering 1 W at 1 MHz output signal frequency using a resonance circuit. A high power Class D Amplifier is proposed in [14] which is also based on a resonant circuit with a rated output power of 1600 W at a resonant frequency of 34.6 kHz.

In summary, it can be stated that the load impedance is critical for the design of the Class D Amplifier. In the publications presented above, a series resonant circuit with well-known properties is used to obtain sinusoidal signals. For the use of the Class D Amplifier in a ripple current generator, this means that the passive elements involved would have to be adapted to the connected load which are the capacitors to be aged.

The discussion of the Class D Amplifier shows that technical useful solutions rely on a series resonant network. So does the proposed solution in [9] where a Series Resonant Converter is commissioned. Analyzing the waveforms given in the publication, it delivers an effective current of at least 5.3 A at 10 kHz. The frequency is determined by the components that form the resonant circuit. That means, that a change in the test frequency makes it necessary to make changes in the used components. This is not a topology-specific drawback because these changes would be necessary for a Class D Amplifier, too.

So the goal is to develop a compact generator that is as easy to modify as possible. With the help of a holistic system approach, rules for dimensioning the resonance components are to be derived to realize test frequencies of interest for the systematic ageing of capacitors. The discussion above requires a wide

frequency range and opportunities to adjust the temperature, humidity, DC voltage and a huge number of DUTs for the sake of modularity.

Table II: Compact Representation of the Topology Study

	<b>Class G Amplifier</b>	<b>Class D Amplifier</b>	<b>Series Resonant Converter</b>
<b>greatest advantage</b>	specifiability of the real current forms	high flexibility by specifying the switching pattern	widely pure sinusoidal currents
<b>greatest drawback</b>	limited dynamics, very high power dissipation	harmonics and EMI due to switching pattern [12], therefore high filter effort	frequency determined by resonant tank, impedances of the transformer, cables, DUTs, ...
<b>current form and maximum test frequency</b>	any (up to 50 kHz)	sinusoidal (MHz range) depending on switching pattern and filter design [13], [14], [15]	sinusoidal (MHz range)
<b>approach</b>	topology-independent induce expected waveforms	topology-independent test frequency components individually	topology-independent test frequency components individually

## V Proposed Approach

Fig. 3 illustrates the proposed approach to consider the ripple current. The current waveforms occurring at the DC-link capacitor in any target topology can be easily decomposed into their spectral components in a circuit simulation. The Fourier Transform then provides information about the occurring current amplitudes over the frequency range of interest.

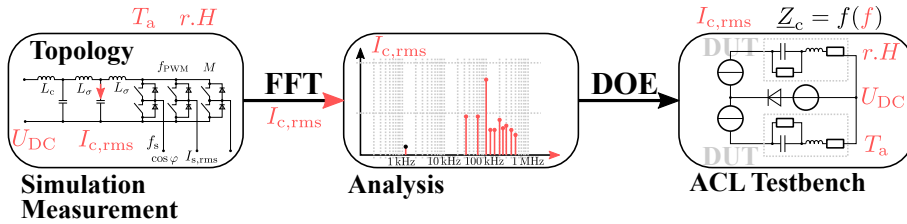


Fig. 3: Methodology of the proposed approach

If sinusoidal currents are generated by the current ripple generator to be developed, the interfering frequencies can be tested individually and their influence on the ageing behaviour of the capacitors can be analyzed. Unlike the push-pull output stage, there is no disturbing distortion of the output signal since here only one frequency is impressed and no superposition of many. In this approach, the generator can stay outside the climatic chamber due to the current sine wave. However, this setup has to cover a wide frequency range for applications with WBG semiconductors, as shown in Fig. 3.

Fig. 4 shows the modular concept. In a ventilated housing, multiple ripple current generators can be operated in the laboratory environment. The devices under test (DUTs) can be placed into a climate chamber where environmental conditions like temperature and humidity can be controlled. The electrical stressors are then provided by the modular ripple current generators.

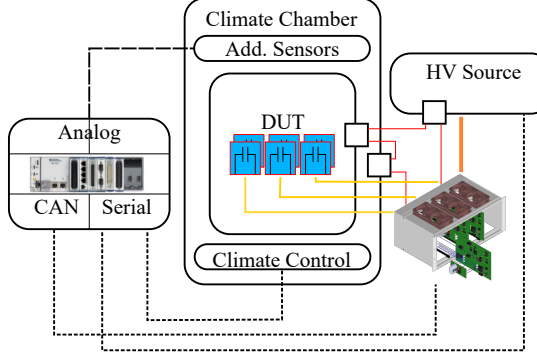


Fig. 4: Proposed modular, topology-independent approach

## VI Design of a modular and flexible Series Resonant Converter

A modular resonant tank is proposed which can realize frequencies in the range of 10 kHz to 500 kHz. Gallium nitride (GaN) semiconductors are used here. With a view to future applications with higher frequencies and due to the low input voltage, these are ideally suited for the design of the ripple current generator. Further requirements are given in Table III.

Table III: Requirements List

<b>transferable power</b>	100 W
<b>maximum effective current</b>	10 A
<b>DUT capacitance range</b>	2 $\mu$ F ... 200 $\mu$ F
<b>frequency range</b>	10 kHz ... 500 kHz

A transformer is needed to connect to the high voltage side where the DUTs are exposed to a voltage of up to 1 kV.

For current regulation, a two-stage approach is used. Using a buck converter, the voltage of the input side can be adjusted in reference to the secondary side current through the DUTs. For this purpose, the current in the resonant circuit is measured and compared with the set reference value. A control algorithm is used to adjust the input voltage of the resonant converter so that the sinusoidal current maintains its amplitude over the entire course of the test. With this approach, a status monitoring of the corresponding circuit can be realized and errors can be reacted to.

## A Subsystem Analysis

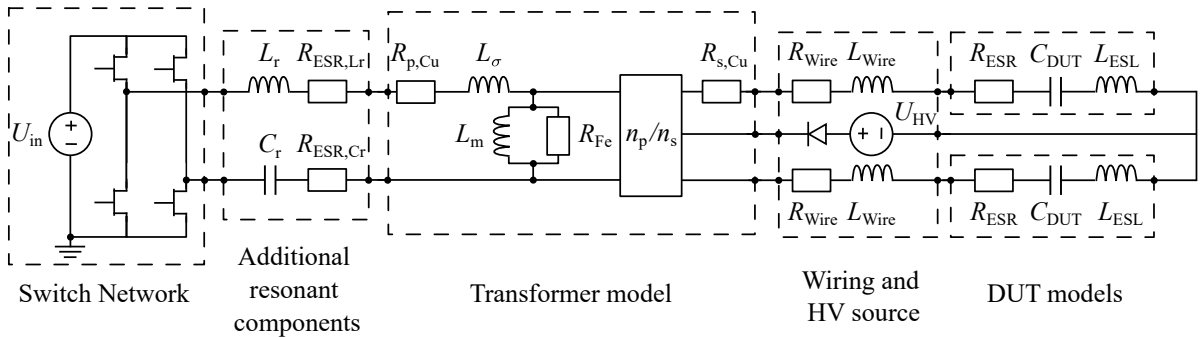


Fig. 5: Circuit model of the ripple current generator

The resonant system consists of five subsystems which are visible in Fig. 5. The input quantity is impressed by the Switch Network with the switching frequency  $f_{sw}$  and the duty cycle  $D = 0.5$ . Using the

First Harmonics Approximation, the input voltage of the resonant system can be calculated with

$$u(t) \approx \frac{4 \cdot U_{\text{in}}}{\pi} \cdot \sin(\omega t) \quad (1)$$

where  $\omega = 2\pi f_{\text{sw}}$ . The system's resonant frequency is dependent on the subsystems consisting of the additional resonant components, the transformer, the wiring and the DUTs. A practical approach for the design of the ripple current generator is to start on the right-hand side of Fig. 5.

This example considers two capacitors connected in series. They can be modelled with their parasitic components so that each DUT is formed by a series connection of the capacitor's equivalent series resistance  $R_{\text{ESR}}$ , the capacitance  $C_{\text{DUT}}$  as well as the equivalent series inductance  $L_{\text{ESL}}$ .

The second subsystem that needs to be considered is the wiring. The primary line constants of the cables used cannot be ignored. In this work, cables are going to be approximated by an ohmic-inductive load. This model is a result of measurements using an impedance analyzer. Two coaxial cables are used for the test fixture. These are specified for the high ambient temperatures and operating voltages. While the inner conductor carries the ripple current in each case, the outer conductors ensure the determination of the potential specified by the voltage source  $U_{\text{HV}}$ .

The transformer also affects the resonant system. This subsystem can be modelled using a simplified equivalent circuit of the transformer that is also given in Fig. 5. Were  $R_{p,\text{Cu}}$  is the ohmic resistance of the primary winding at a given frequency. The leakage inductance  $L_{\sigma}$  contributes dominantly to the properties of the resonant circuit. With decreasing transformer size also the magnetizing inductance  $L_m$  decreases. When  $L_{\sigma}$  and  $L_m$  are in the same order of magnitude, the magnetizing current cannot be neglected. Thus, especially for higher frequency ranges, the magnetizing inductance  $L_m$  needs to be considered. On the transformer's secondary side there  $R_{s,\text{Cu}}$  is the ohmic resistance of the secondary winding.

Lastly, there are the additional resonant components that are modelled in Fig. 5. Because the other components that contribute to the overall resonant frequency are fixed by the properties of the used subsystems (DUTs, wiring and transformer) the additional resonant components are being used to tune the resonant frequency to the desired value.

## B Reducing the complexity of the model and formulation of design rules

The complex system shown in Fig. 5 can be transformed into a more compact one if related elements and impedances are combined at suitable points. This summary of the components is shown in Fig. 6 for the subsystems to the right of the Switch Network. Here, secondary-side impedances  $Z_s$  are taken into

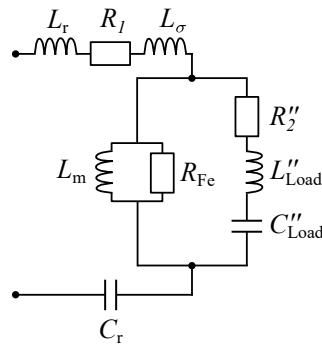


Fig. 6: Equivalent circuit of the resonant circuit

account by the transformation

$$Z_s'' = \left( \frac{n_p}{n_s} \right)^2 \cdot Z_s \quad (2)$$

on the primary side using the number of primary turns  $n_p$  as well as the number of secondary turns  $n_s$ . With all relevant resonance frequency-determining elements identified, the network model given in Fig. 6

can be derived. Analyzing the overall impedance of the network model and taking into account that at the resonance frequency the imaginary part of the impedance needs to be zero the resonance frequency can be calculated using

$$f_{\text{res}} = \frac{1}{2\pi\sqrt{\left(L_r + L_\sigma + \frac{L''_{\text{Load}} \cdot L_m}{L''_{\text{Load}} + L_m}\right) \cdot \frac{C_r C''_{\text{Load}}}{C_r + C''_{\text{Load}}}}} \quad (3)$$

At resonance frequency, only the purely real, ohmic resistance

$$R_{\text{sum}} = R_1 + R''_2 \quad (4)$$

is still effective when the losses in the core materials are neglected by stating  $R_{\text{Fe}} \rightarrow \infty$ . With the target frequency  $f_{\text{target}}$  and using the definition of the quality factor

$$Q_{\text{target}} = \sqrt{\frac{L_{\text{target}}}{C_{\text{target}}}} \cdot \frac{1}{R_{\text{sum}}} \quad (5)$$

the target values of the overall equivalent inductance  $L_{\text{target}}$  and capacitance  $C_{\text{target}}$  can be calculated using

$$L_{\text{target}} = \frac{1}{2\pi f_{\text{target}}} \cdot (Q \cdot R_{\text{sum}})^2 \quad (6)$$

respectively

$$C_{\text{target}} = \frac{1}{2\pi f_{\text{target}}} \cdot \frac{1}{(Q \cdot R_{\text{sum}})^2} \quad (7)$$

The values of the additional resonant components  $L_r$  and  $C_r$  that need to be placed into the resonant path are determined by

$$L_r = L_{\text{target}} - L_\sigma - \frac{L''_{\text{Load}} \cdot L_m}{L''_{\text{Load}} + L_m} \quad (8)$$

as well as

$$C_r = \frac{C_{\text{target}} \cdot C''_{\text{Load}}}{C''_{\text{Load}} - C_{\text{target}}} \quad (9)$$

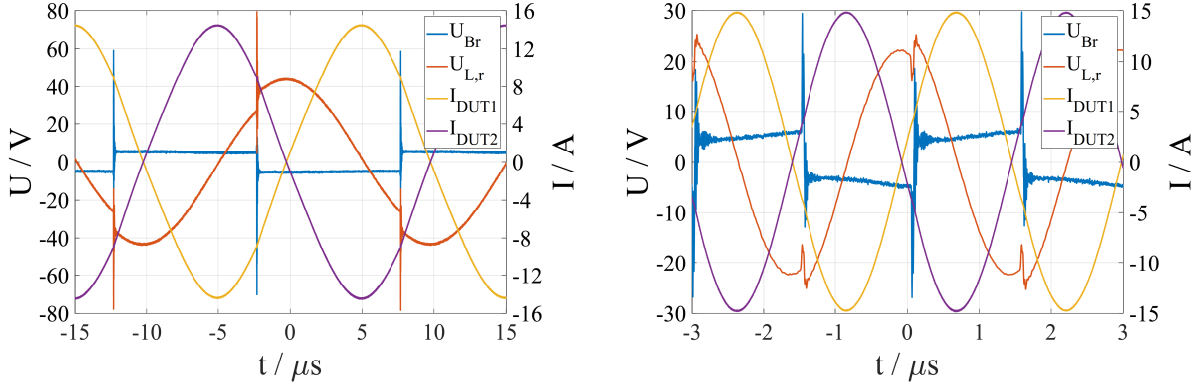
where  $L_r, C_r \geq 0$  must be fulfilled.

## VII Experimental setup



Fig. 7: Modular ripple current generator with adapter boards

Fig. 7 shows the developed ripple current generator with adapter boards to set the resonant frequency using  $L_r$  and  $C_r$ . These adapter boards also carry the transformer. The proof of function is to be shown



a) Waveforms of the 50kHz resonance circuit with planar transformer      b) Waveforms of the 327kHz resonance circuit with conventional transformer

Fig. 8: Waveforms captured during the commissioning of the proposed ripple current generator

for two frequencies. The first frequency is  $f_1 = 50\text{kHz}$  which is the fundamental frequency in the example application of the three-phase inverter. The second frequency  $f_2 = 327\text{kHz}$  is the self-resonance frequency of the DUTs which were previously identified using an impedance analyzer.

Three transformers are designed and used in this work from which one is a planar transformer. With a small number of transformers with well known properties, a high degree of modularity can be achieved. The researcher can choose the right component from a well documented pool of transformers. In this context, the planar transformer can significantly contribute to a further increase in modularity. Challenges arise concerning the development time of such a device. The benefits are the repeatability and multiple ways of the winding realization.

An oscillogram with measured quantities on the 50kHz circuit is given in Fig. 8a. The measured quantity  $U_{Br}$  is the voltage at the input terminals of the resonant circuit shown in Fig. 6. The voltage  $U_{L,r}$  is the voltage across the resonance inductor, while  $I_{DUT1}$  and  $I_{DUT2}$  are a representation of the current through the capacitors to be aged. While  $I_{DUT1}$  flows out of the ripple current generator,  $I_{DUT2}$  is the current flowing back into the device. Because of the planar transformer's direction of winding the positive half-wave of  $I_{DUT1}$  appears during the period where  $U_{Br}$  is negative.

Fig. 8a shows sinusoidal currents through the capacitors to be aged. Analyzing the current's amplitude, the goal to imprint an effective current of 10 A is achieved.

The voltages shown in Fig. 8a exhibit high voltage peaks at the switching moment, accompanied by oscillations. These are significantly favoured by two circumstances.

First, it can be seen that the resonant frequency of the system does not match the switching frequency completely. Component tolerances, which also drift over the temperature, are primarily responsible for this.

The second reason is associated with the semiconductor switches used. The GaN switches exhibit a very steep switching behaviour and challenging reverse conduction characteristics when reverse biased [16]. This favours the observed behaviour. As a result, additional losses occur in the inductor, but these can be well controlled with the measures taken.

In conclusion, it can be stated that the voltage stress on the components, which is determined by  $Q$ , is in the expected range. Thermal tests show that the ripple current generator and the designed resonance circuits are thermally safe for continuous operation.

The commissioning of the 327kHz resonance circuit shows similar behaviour. Fig. 8b shows sinusoidal currents with an effective current of 10A. Because the resonance frequency of the resonant circuit is closer to the switching frequency, the voltage peaks at the switching moment are lower in their amplitude. This leads to lowered losses in the inductor. Thus, this resonance circuit is thermally safe for continuous operation, too.

## VIII Experimental results

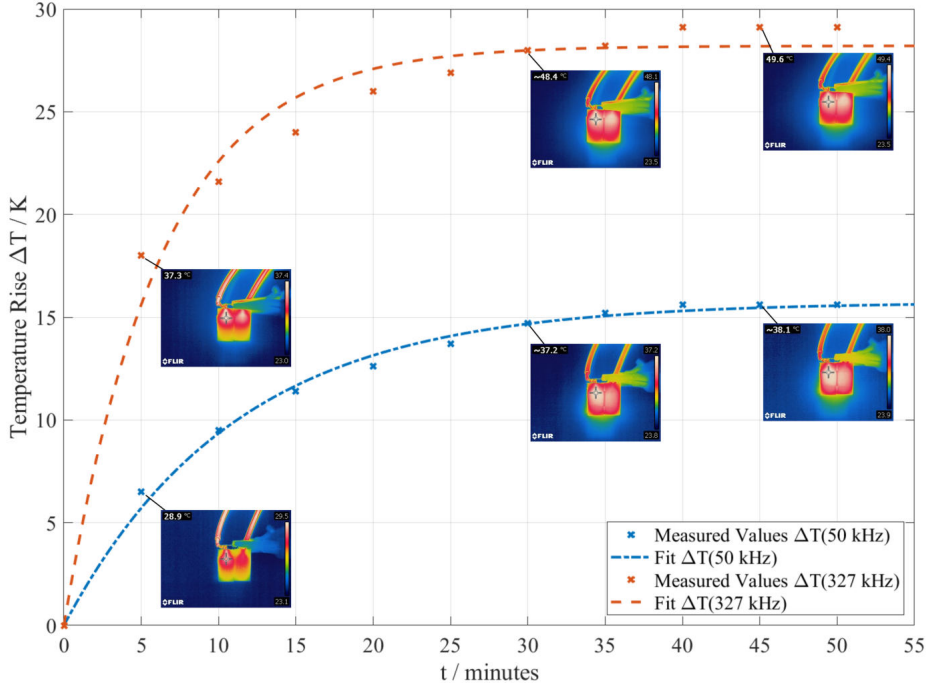


Fig. 9: Temperature rise of the tested capacitor at two different test frequencies

During commissioning, it is observed that the capacitors heat up to different degrees depending on the frequency of the ripple current, as shown in Fig. 9. At a frequency of 50kHz, they heat up by 15.7K compared to room temperature, while at 327kHz a heating of 28.2K is detectable. The temperature is measured in each case with the aid of a thermal imaging camera. The capacitor's thermal time constant is  $\tau \approx 11.1$  min. For future investigations at further frequencies, a more suitable measurement method must be selected. For example, thermocouples can be used here, which may be attached to the capacitors.

## IX Conclusion

Reliable electrical drive and supply systems for aviation are getting more and more important. New developments make use of fast-switching WBG semiconductors. Thus, new approaches must be found to determine the reliability and service life of capacitors which are exposed to a harsh environment and high frequent ripple currents of rising frequencies. For this purpose, they have to be systematically subjected to a ripple current under fixed (climatic and electrical) conditions. This arises the need for modular and compact systems for accelerated ageing of capacitors in higher frequency ranges. Current publications and standards do not provide a satisfactory solution for this issue. This paper addresses some approaches to accelerated ageing of capacitors known from the literature. For the generation of high-frequency sinusoidal ripple currents, dimensioning rules of a modular ripple current generator based on a resonant converter are presented. The ripple current generator dimensioned with these rules is presented and its commissioning is documented.

## References

- [1] H. Schefer, L. Fauth, T. H. Kopp, R. Mallwitz, J. Fribe and M. Kurrat, "Discussion on Electric Power Supply Systems for All Electric Aircraft," in IEEE Access, vol. 8, pp. 84188-84216, 2020, <https://doi.org/10.1109/ACCESS.2020.2991804>
- [2] S. Yang, A. Bryant, P. Mawby, D. Xiang, L. Ran and P. Tavner, "An industry-based survey of reliability in power electronic converters," 2009 IEEE Energy Conversion Congress and Exposition, 2009, pp. 3151-3157, <https://doi.org/10.1109/ECCE.2009.5316356>

- [3] H. Wang, H.Wang, Z. Shen, "Reliability of Capacitors and Magnetic Components in Power Electronic Applications," in CIPS 2020; 11th International Conference on Integrated Power Electronics Systems, 2020, pp. 1-6, <https://ieeexplore.ieee.org/document/9097729>, accessed: 17.11.2021
- [4] H. Wang and F. Blaabjerg, "Reliability of Capacitors for DC-Link Applications in Power Electronic Converters—An Overview," in IEEE Transactions on Industry Applications, vol. 50, no. 5, pp. 3569-3578, Sept.-Oct. 2014. <https://doi.org/10.1109/TIA.2014.2308357>
- [5] Nippon Chemi-Con Corporation, "Judicious use of aluminium electrolytic capacitor," Technical Note, <https://www.chemi-con.co.jp/e/catalog/pdf/al-e/al-sepa-e/001-guide/al-technote-e-2020.pdf>, accessed: 12.11.2021
- [6] M. Makdessi, A. Sari, P. Venet, "Metallized polymer film capacitors ageing law based on capacitance degradation", Microelectronics Reliability, Volume 54, Issues 9–10, 2014, Pages 1823-1827, ISSN 0026-2714, <https://doi.org/10.1016/j.microrel.2014.07.103>.
- [7] W. Minford, "Accelerated Life Testing and Reliability of High K Multilayer Ceramic Capacitors," in IEEE Transactions on Components, Hybrids, and Manufacturing Technology, vol. 5, no. 3, pp. 297-300, September 1982, <https://doi.org/10.1109/TCHMT.1982.1135974>
- [8] J.W. Kolar, S.D.Round, "Analytical calculation of the RMS current stress on the DC-link capacitor of voltage-PWM converter systems", IEEE Proceedings - Electric Power Applications, Volume 153, Issue 4, Pages 535-543, ISSN 1359-7043, <https://doi.org/10.1049/ip-epa:20050458>
- [9] M. Makdessi, A. Sari, P. Venet, P. Bevilacqua, C. Joubert, "Accelerated Ageing of Metallized Film Capacitors Under High Ripple Currents Combined With a DC Voltage," in IEEE Transactions on Power Electronics, vol. 30, no. 5, pp. 2435-2444, May 2015, <https://doi.org/10.1109/TPEL.2014.2351274>
- [10] C. Kulkarni, G. Biswas, X. Koutsoukos, J. Celaya, and K. Goebel, "Experimental Studies of Ageing in Electrolytic Capacitors," in Annual Conference of the Prognostics and Health Management Society, Portland, OR, October 2010, <https://citeseerx.ist.psu.edu/viewdoc/download?doi=10.1.1.300.1607&rep=rep1&type=pdf>, accessed: 15.11.2021
- [11] K. Hasegawa, I. Omura and S. -i. Nishizawa, "A new evaluation circuit with a low-voltage inverter intended for capacitors used in a high-power three-phase inverter," 2016 IEEE Applied Power Electronics Conference and Exposition (APEC), 2016, pp. 3032-3037, <https://doi.org/10.1109/APEC.2016.7468295>
- [12] Douglas Self. Audio power amplifier design handbook. 3. ed., reprinted. Amsterdam: Newnes, 2003. ISBN: 0750656360.
- [13] S.-A. El-Hamamsy, "Design of high-efficiency RF Class-D power amplifier," in IEEE Transactions on Power Electronics, vol. 9, no. 3, pp. 297-308, May 1994, <https://doi.org/10.1109/63.311263>
- [14] H. Koizumi, T. Suetsugu, M. Fujii, K. Shinoda, S. Mori and K. Ikeda, "Class DE high-efficiency tuned power amplifier," in IEEE Transactions on Circuits and Systems I: Fundamental Theory and Applications, vol. 43, no. 1, pp. 51-60, Jan. 1996, <https://doi.org/10.1109/81.481461>
- [15] N. -J. Park, D. -Y. Lee and D. -S. Hyun, "A Power-Control Scheme With Constant Switching Frequency in Class-D Inverter for Induction-Heating Jar Application," in IEEE Transactions on Industrial Electronics, vol. 54, no. 3, pp. 1252-1260, June 2007, <https://doi.org/10.1109/TIE.2007.892741>
- [16] E. A. Jones, F. F. Wang and D. Costinett, "Review of Commercial GaN Power Devices and GaN-Based Converter Design Challenges," in IEEE Journal of Emerging and Selected Topics in Power Electronics, vol. 4, no. 3, pp. 707-719, Sept. 2016, <https://doi.org/10.1109/JESTPE.2016.2582685>